Opt Quant Electron (2012) 43:69–82
DOI 10.1007/s11082-011-9504-5

Investigation on parameters affecting the performance of two dimensional photonic crystal based bandpass filter

S. Robinson · R. Nakkeeran

Received: 5 February 2011 / Accepted: 5 November 2011 / Published online: 20 November 2011

Abstract A two dimensional Photonic Crystal based Bandpass Filter is designed by exploiting coupling between the quasi waveguides and the circular Photonic Crystal Ring Resonator (PCRR). The output efficiency, resonant wavelength and bandwidth of PCBPF are investigated by varying the dielectric constant of the structure. The normalized transmission spectra of circular PCRR are taken using 2D Finite Difference Time Domain method. The Photonic Band Gap is calculated by Plane Wave Expansion method. Close to 100% (Band II) output efficiency is observed over the wavelength range from 1,504 to 1,521 nm and 85% (Band I) is obtained at 1,420 nm through simulation. The full width half maximum bandwidth of these bands is 35 and 20 nm, respectively. Further, the parameters that affect the resonant wavelength, output efficiency and bandwidth of the filter such as size of the reflector, radius of the coupling rods, lattice constant, rod radius and number of rods in the structure are analyzed. The overall size of the proposed filter is $11.4\,\mu\text{m} \times 10.2\,\mu\text{m}$, which is smaller than the filters already reported in the literature and highly desirable for Photonic Integrated Circuits.

Keywords Photonic crystal ring resonator · Photonic band gap · Photonic integrated circuits · Bandpass filter · FDTD method · PWE method

1 Introduction

The miniaturization of the optical devices with high speed, long life and less power dissipation is one of the pioneering research areas. The Planar Lightwave Circuits (PLC) and Micro-electromechanical Systems (MEMS) have been playing a crucial role for optical device miniaturization. Generally, the PLC based devices are in the order of centimeters (Shih et al. 2009). The MEMS based devices at the order of micrometer dimension prone to radiation and bending losses which lead to sensitivity deterioration at higher speed. Also, this technique

S. Robinson (✉) · R. Nakkeeran
Department of Electronics and Communication Engineering,
Pondicherry Engineering College, Puducherry 605 014, India
e-mail: mail2robinson@pec.edu

results in lower life period owing to movable components (Qiang et al. 2007). Hence, it may not be effectively suitable for Photonic Integrated Circuits (PICs). The above mentioned issues can be solved by designing the devices using Photonic Crystals (PCs).

Very promising ultra compact devices for integrated optics can be obtained by composing PCs. Generally, PCs are patterned artificial materials with periodicity of dielectric constant in one, two or three dimensions, which can create a range of forbidden frequencies called Photonic Band Gap (PBG). It is the range of wavelength for which material neither absorbs nor allows the light propagation inside the structure (Yablonovitch 1987; John 1987; Joannopoulos et al. 1995, 1997). The completeness of the periodicity can be disturbed by introducing defects and hence PBG, which allows the guided modes to propagate inside this region. The existence of PBG in PCs is more suitable for designing optical devices.

In recent years, many PC based optical devices have been discussed theoretically and experimentally such as add-drop filters (Qiang et al. 2007; Robinson and Nakkeeran 2011b), power splitters (Nozhat and Granpayeh 2007; Ghaffari et al. 2008a), channel drop filters (Hwang and Song 2005; Djavid et al. 2008b; Wang et al. 2010; Robinson and Nakkeeran 2010), multiplexers and demultiplexers (Manzacca et al. 2007; Ghaffari et al. 2008b), polarization beam splitters (Liu et al. 2005; Zabelin et al. 2007), triplexers (Park et al. 2008; Shih et al. 2009), switches (Wang et al. 2010), directional couplers (Moghaddam et al. 2010), bandstop filters (Monifi et al. 2008), bandpass filters (Costa et al. 2003; Chao et al. 2007; Djavid et al. 2008a; Robinson and Nakkeeran 2011a) and so on.

Essentially, optical filter is one of the prominent components in Wavelength Division Multiplexing (WDM) system, which multiplexes many channels and fed into a fiber. Therefore, Bandpass Filter (BPF) is necessary to select a single or multiple channels from the WDM systems. In the literature, BPF has been designed by introducing point defects and/or line defects (Costa et al. 2003; Chao et al. 2007), and using biperiodic structures (Djavid et al. 2008a). Moreover, the authors have not seen any other method of designing PC based BPF in the literature till date. Since the waveguide coupled ring resonator based optical devices could provide better selectivity, scalability and flexibility in mode design (Qiang et al. 2007), in this paper an attempt is made to design the Ring Resonator based BPF using pillar type (rod/air) PCs. Typically, pillar based PCs have several advantages such as low out-of-plane losses, propagation loss, easy fabrication, compatible with classical PICs, and effective single mode operation due to defects based structure. (Kok et al. 2009). Two dimensional (2D) PCs are receiving keen attention by the scientific community as they have attractive features including relatively simple fabrication, better confinement of light, efficient PBG calculation, effective control of spontaneous emission and easy integration with other devices (Joannopoulos et al. 1995). Owing to the above advantages, authors conceived 2D pillar type PC for BPF design.

In this paper a 2D-PCBPF by using circular Photonic Crystal Ring Resonator (PCRR) is designed and investigated. The output efficiency and resonant wavelength are examined by varying the dielectric constant of the structure. We further considered the effect of variation of dielectric constant of inner and outer rods, size of the reflector, radius of the coupling rods, lattice constant, rod radius and number of rods in the structure to determine the above said parameters. Simulation of the designed filter is carried out by 2D Finite Difference Time Domain (FDTD) method. The Plane Wave Expansion (PWE) method is employed to calculate PBG of the filter with and without defects using band diagram. The FDTD and PWE methods are simulated using Fullwave and Bandsolve simulator of Rsoft.

The rest of the paper is arranged as follows: In Sect. 2, the band diagram, gap map and structure design of circular PCRR are presented. Simulation results are discussed in Sect. 3. In Sect. 4, numerical analysis of the parameters affecting the performance of the filter is enumerated and Sect. 5 concludes the paper.

2 Structure design

The perfect square lattice periodic PC structure is considered for designing PCBPF, which consists of 21 and 19 rods in 'X' and 'Z' directions, respectively. The radius of the rod, r is $0.185 \times$ a (0.1 μm), where 'a' is the distance between any two nearest rods, called as lattice constant. The dielectric constant of the rod is 12 (refractive index, 'n' is 3.4641), which corresponds to the effective index of Si rods embedded in air host. The lattice constant is chosen to be 540 nm to design PCBPF.

The Fig. 1a shows the first Brillouin zone of the square lattice. The band diagram (1×1 PC i.e., unit cell) reveals the PBG region and the electromagnetic waves that propagate inside the periodic PC structure are shown in Fig. 1b where two TM (Transverse Magnetic) PBGs (blue region) are identified. It shows the frequency of first reduced PBG from 0.295 a/λ to 0.435 a/λ whose corresponding wavelength range accounts from 1,241 to 1,830 nm and second PBG from 0.732 a/λ to 0.754 a/λ whose corresponding wavelength range lies from 716 to 737 nm. Here, TM polarization is considered as the PC has PBG exclusively for the TM polarization alone in which the electric field is parallel to the rod axis and the magnetic field is perpendicular to the rod axis. The guided modes (even or odd) propagate inside the first TE PBG region due to the introduction of line and point defects (21×19 PC i.e., super cell) are shown in Fig. 1c.

The gap map shown in Fig. 2a–c represent the variation of TE/TM PBG with the variation of radius of the rod, lattice constant (period) and refractive index (delta) difference. These values, which are used to design the PCBPF, are chosen from the gap map so as to cover the entire first reduced TM PBG. The verical and horizondal axes of the gap map are

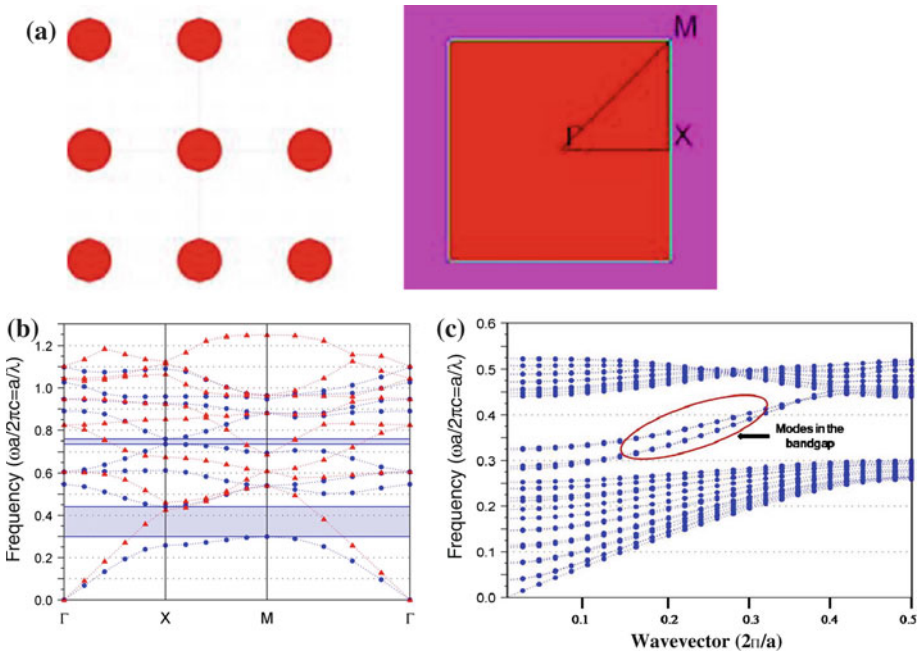

Fig. 1 **a** Brillouin zone of square lattice, **b** band diagram of 1×1 PC (unit cell) and **c** 21×19 PC (super cell) square lattice structure after the introduction of line and point defects (guided modes inside the PBG region)

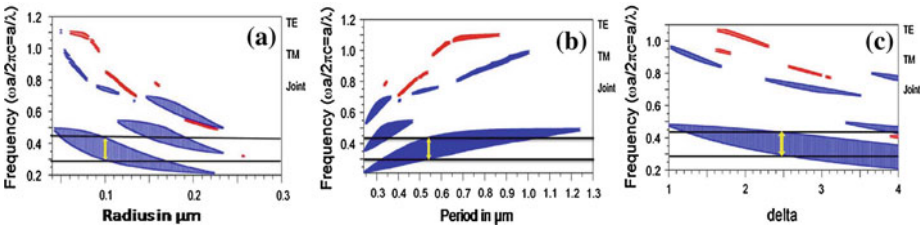

Fig. 2 Effect of TE/TM PBG by varying **a** radius of the rod, **b** period (lattice constant) and **c** delta (index difference)

frquency (a/λ) and structural parameters (radius of the rod, period and delta), respectively. In these figures, the blue region indicates the variation of TM PBG with respect to radius of the rods, period and delta similarly the red region indicates the effect of TE PBG. The vertical yellow line over blue region represents TM BPG region (0.295 a/λ to 0.435 a/λ) of the structure without any defects. The values to design the PCBPF in the first reduced TM PBG are optimized through gap map. They are, rod radius (0.1 μm), refractive index (3.4641) and period (540 nm) as indicated in the gap map. 2D-FDTD method is used to simulate the PC structure and Perfect Matched Layer (PML) is placed as absorbing boundary condition (Berenger 1994; Lavrinenko et al. 2004) around the structure.

Figure 3a, b sketch the schematic structure of circular resonant cavity and the circular PCRR based BPF. The PCBPF consists of two quasi waveguides in horizontal (Γ-x) direction and a circular PCRR between them. The input Gaussian signal is applied to the port marked 'A' (arrow in the left side of top quasi waveguide) and the output is detected using power monitor which is positioned at the output port marked 'B' (arrow left side of the bottom quasi waveguide). The rods inside the circular PCRR are called as inner rods. The coupling rod is placed between circular PCRR and quasi waveguides, marked as 'c'. The reflectors, demarcated in rectangular box, placed above and below the right side of circular PCRR are shown in Fig. 3b, which are used to improve the output efficiency of the PCBPF by reducing the counter propagation modes. In order to enhance the output efficiency and maintain the structure in symmetric nature, the number of periods (Si rods) in the reflector is kept constant, 9. Figure 3c clearly pictures the three dimensional (3D) view of the device and its overall size comes around 11.4 μm × 10.2 μm.

3 Simulation results

A Gaussian input signal is launched into the input port 'A'. The normalized transmission spectra shown in Fig. 4a are obtained at port 'B' by conducting Fast Fourier Transform (FFT) of the fields that are calculated by 2D-FDTD method. The input and output signal power is recorded by power monitors which are positioned at the input and output ports. The normalized transmission is calculated through the following formula

$$T(f) = \frac{1/2 \int real(p(f)^{monitor})\, dS}{SourcePower}$$

where $T(f)$ is a normalized transmission as a function of frequency, $P(f)$ is a pointing vector and dS is the surface normal. The further normalization at the output side does not affect the result because of the source power normalization.

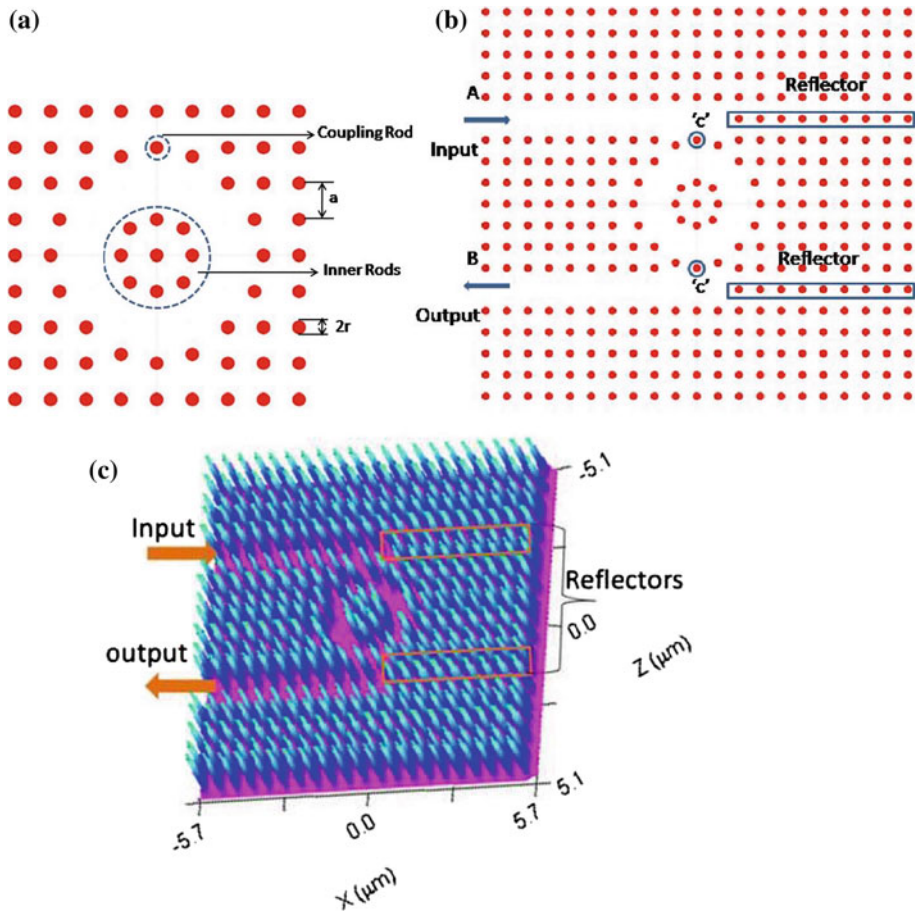

Fig. 3 Schematic structure of **a** circular resonant cavity, **b** 21 × 19 circular PCRR based BPF and **c** three dimensional view of BPF

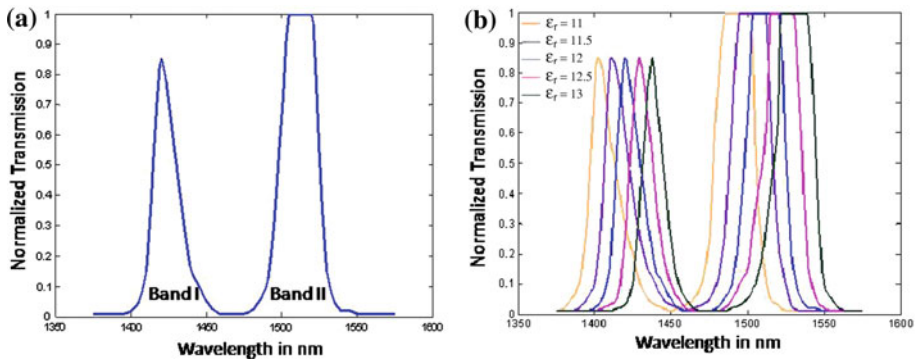

Fig. 4 Normalised transmission spectra of **a** circular PCRR based BPF and **b** variation in dielectric constant ($\varepsilon_r = 11$, $\varepsilon_r = 11.5$, $\varepsilon_r = 12$, $\varepsilon_r = 12.5$ and $\varepsilon_r = 13$)

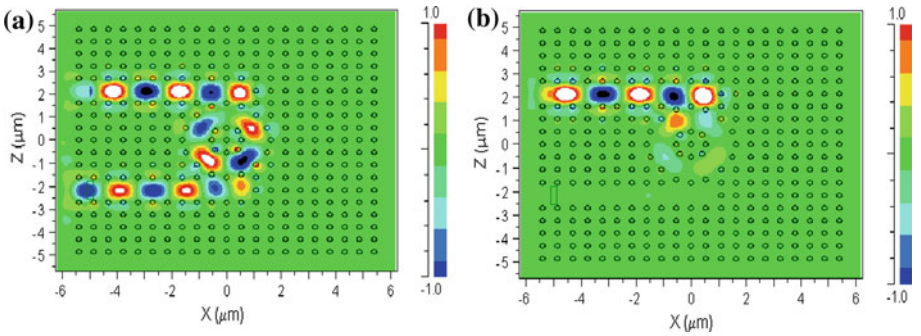

Fig. 5 Electric field pattern of circular PCRR based BPF with the coupling rod radius 0.1 μm at: **a** 1,512 nm and **b** 1,550 nm

The observed output efficiency is approximately 85% at 1,420 nm and close to 100% over the range of wavelengths 1,504–1,521 nm whose corresponding bands are denoted as Band I and Band II, respectively. The center wavelength and Full Width Half Maximum (FWHM) bandwidth of these bands are 1,420, 1,512.5, 20, and 35 nm, respectively. Also, the calculated Q factor of Band I and Band II is 71 and 50.41, respectively. As it is witnessed in the previous work (Robinson and Nakkeeran 2011a,b), the number of passbands depends on the number of inner rings that are formed by the inner rods. Here, the considered two inner rings result two passbands. The size and shape of the ring resonator determines the resonant wavelength. The bandwidth and channel spacing are decided by the other structural parameters such as radius of the rod, period and dielectric constant (refractive index) of the material.

In general, the refractive index is equal to the square root of relative permittivity of the given medium. The relative permittivity can also be called as dielectric constant of that medium and hence, the dielectric constant is used here instead of refractive index. The Fig. 4b illustrates the relation between the output efficiency and wavelength shift for different dielectric constant of the structure. It clearly explains that the center wavelength of the bands shift into the lower wavelength region (higher wavelength) when the dielectric constant of structure is decreased (increased). It is also noticed that the output efficiency is not significantly changed while varying the dielectric constant of the structure. The magnitude of the wavelength shift is around 9 nm for every 0.5 value change in dielectric constant of the structure. However, the bandwidth is almost not affected by the variation of dielectric constant.

The Fig. 5a, b depict the electric filed pattern of pass region and stop region at 1,512 and 1,550 nm respectively. At resonance, $\lambda = 1{,}512$ nm, the electric field of the waveguide is fully coupled into the ring and reached its output port, whereas at off resonance, $\lambda = 1{,}550$ nm, it is not coupled into the ring i.e., signals are reflected to the counter direction. Hence, the signal does not reach the output resulting in reduced output power.

4 Study of parameters affecting the performance of the filter

In this section, the effect of parameters that are affecting the performance of the PCBPF are discussed in detail. The study of change in resonant wavelength, output efficiency and bandwidth of the filter are inevitable as the filter parameters are unique for different applications. Change in the filter characteristics to a desired level can be obtained by pertuberating one or more of the following structural parameters in a controlled manner:

- Dielectric constant
- Size of the reflector
- Coupling rod radius
- Lattice constant and rod radius, and
- Number of rods in the structure.

The effect of above mentioned parameters for the designed PCBPF is discussed elaborately one by one in the following sections.

4.1 Effect of dielectric constant

To examine the behaviour of resonant wavelength and ouptut efficiency while varying the dielectric constant, the simulation is carried out for different values of dielectric constant of structure, inner rods and outer rods of the circular PCRR. It is observed that, when the dielectric constant of the structure is increased (decreased) by 0.5, the resonant wavelength shifts into the higher wavelength region (lower wavelength) by 9 nm both in Band I and Band II, which is shown in Fig. 6a and the output efficiency is shown in Fig. 6b. It is inferred that the output efficiency of Band II does not change while varying the dielectric constant. However, dielectric constant value change affects the output efficiency of Band I.

For understanding the impact of change in dielectric constant of inner and outer rods, $\varepsilon_r = 12$ is chosen as reference value. When the dielectric constant of the inner rods, outer rods and both are increased (decreased) by 0.5, the resonant wavelength shifts into the higher wavelength (lower wavelength) region by, approximately, 4, 5 and 7.5 nm, respectively as shown in Fig. 6c, e, g whose corresponding output efficiencies are shown in Fig. 6d, f, h.

For smaller dielectric constant value of the structure, the incoming signals scattered around the quasi waveguides and circular PCRR resulting in reduced signal power at output port and hence the output efficiency. The efficiency at higher value of dielectric constant is not affected due to high confinement of light in the defected region of the structure, hence, the maximum amout of power reached to the output port. Moreover, the bandwidth of Band I and Band II is not significantly affected by dielectric constant variation and also the resonant wavelength shift depends on the effective dielectric constant of the PC structure.

4.2 Effect of reflector size

To study the effect of reflector, the simulation is carried out by varying the radius of the rods, the number of rods, increasing the radius of the 1st, 2nd and 3rd rods alone near the cavity and reducing the number of Si rods towards the cavity, of the reflector.

The number of Si rods in the reflector above and below the cavity is kept '9' for maximum power transmission from input to output at resonance. The reflector period represents number of Si rods in the reflector. Initially, the radius of the rods in reflector is varied and the behavior of output efficiency of Band I and Band II is noted. Figure 7a shows that the output efficiency of Band I is reduced while reducing the radius of the rod in the reflector below 0.9 μm. However, Band II is not affected. When the radius of the rod is below 0.05 μm, the signal is scattered through reflector and above 1.5 μm each rods in the reflector is acting as a cavity that results in reduction of output efficiency of both Band I and Band II.

Figure 7b depicts the variation of normalized transmission with respect to reflector periods. If the reflector period is above reference value i.e., greater than '9', it covers both top and bottom of the circular PCRR. Hence, the entire input signal could not couple into the cavity since it is scattered before it reaches the cavity. Similarly, when the reflector

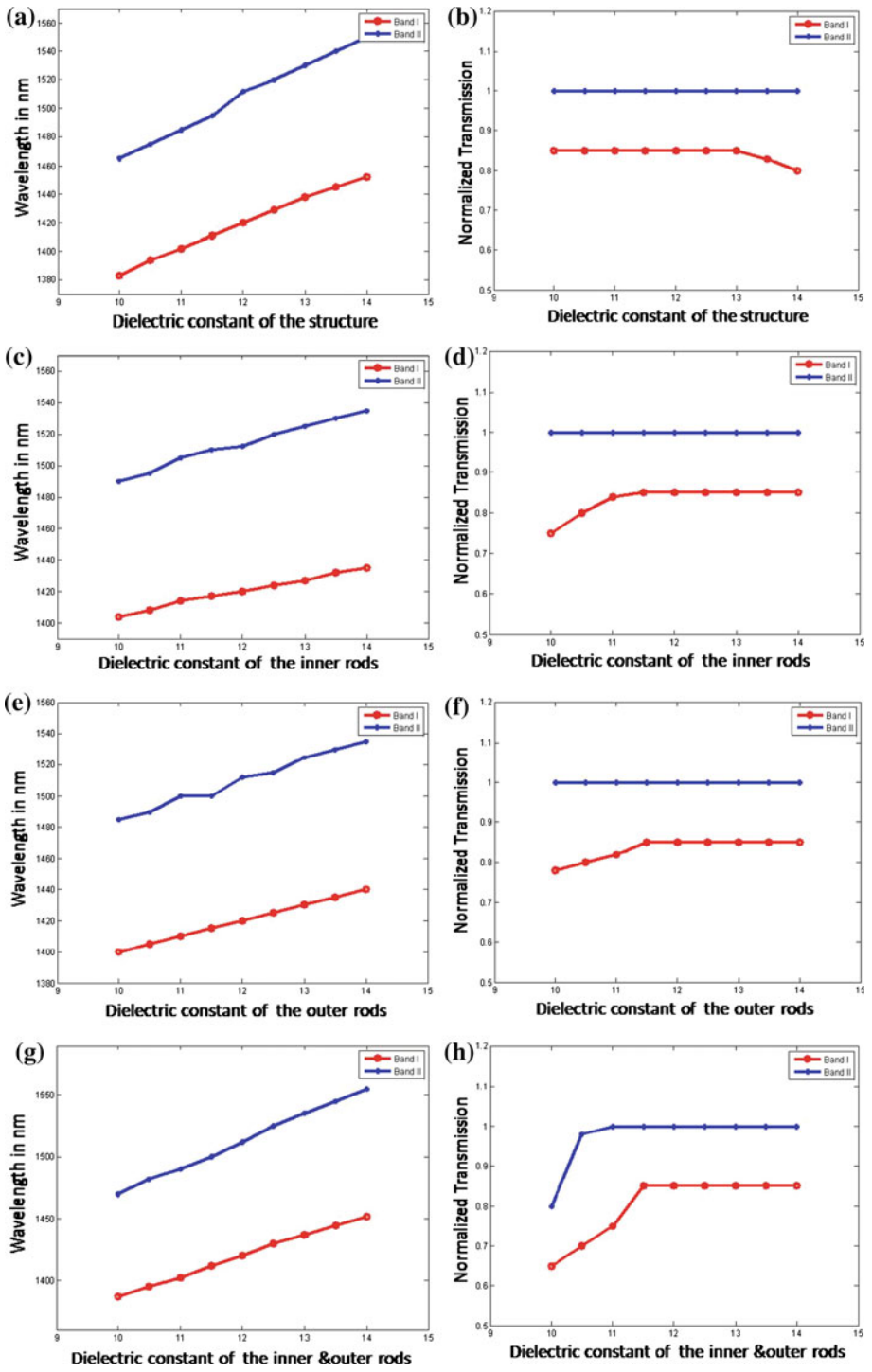

Fig. 6 Effect of resonant wavelength and normalized transmission by varying dielectric constant of: **a**, **b** structure, **c**, **d** inner rods, **e**, **f** outer rods, and **g**, **h** both inner and outer rods

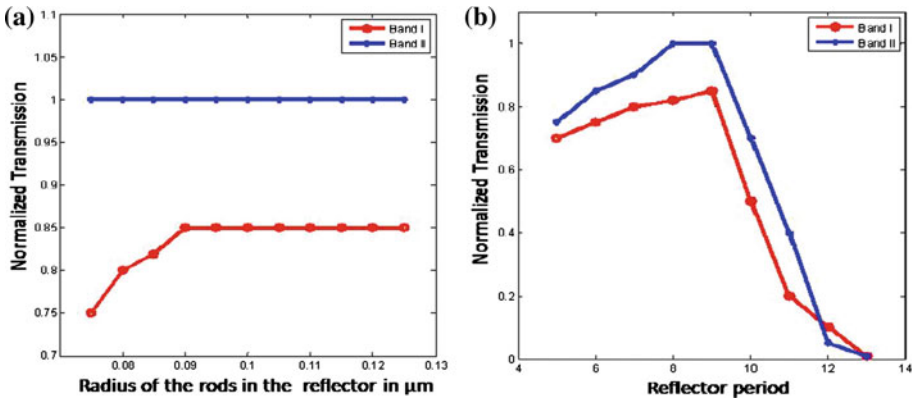

Fig. 7 **a** Output power with respect to the radius of the rods in the reflector, **b** output power with respect to the reflector period

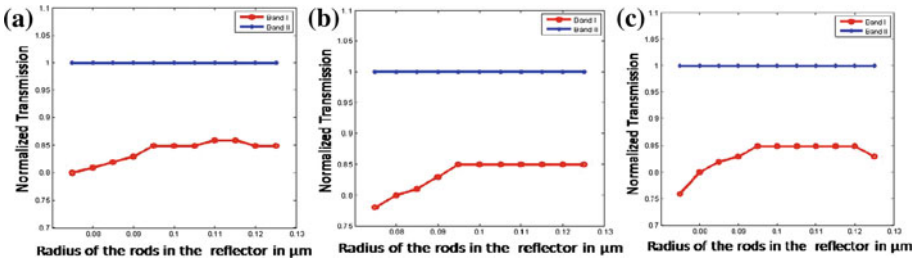

Fig. 8 Output power with respect to radius of the rods **a** 1st rod, **b** 2nd rod and **c** 3rd rod towards the right side

period is below 9, certain amount of power is dropped near the reflector (after the cavity). For 9 Si rods, the reflector is placed such that it is near the coupling rod which is used to reflect the entire incoming signal into the cavity as a result, the maximum power transmission takes place at resonance compared with other periods of the reflector. Hence, it is understood that the initial position of the reflector must be at 2nd rod from the center towards the right side.

The output efficiency with respect to variation of radii of one, two and three rods towards the right side is shown in Fig. 8a–c, respectively. However, Band I output efficiency is reduced when the radius of the rod is reduced below 0.09 μm. It is noted that, the change in rod radius has not contributed substantial improvement in the performance.

Finally, to identify the minimum number of rods required for the reflector to maintain the sufficient output efficiency is done by reducing the number of rods towards the cavity. It is observed that the reduction in number of rods (below 3) in the reflector reduces the output efficiency as shown in Fig. 9. From the above simulation study, it is found that the radius of the reflector is 0.1 μm. The minimum number of Si rods required to meet the acceptable performance is 3. To maintain the symmetric nature, authors used 9 Si rods in the reflector with 0.1 μm rod radius.

4.3 Effect of coupling rod radius

While varying coupling rod radius from 0.1 μm the output efficiency decreases, however, the resonant wavelength is not affected by the variation of coupling rod radius. For variation

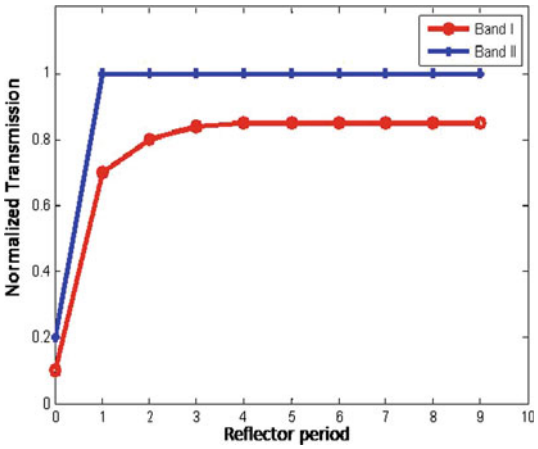

Fig. 9 Output power spectra with respect to the reduction of reflector period towards the cavity

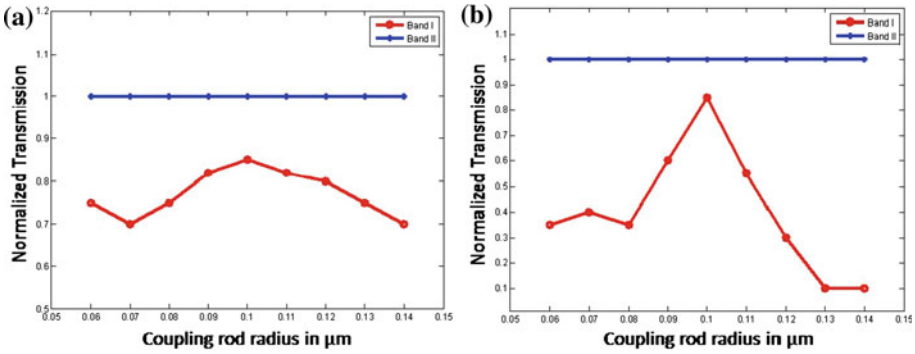

Fig. 10 Effect of output efficiency by varying **a** single and **b** three coupling rod radius

of the radius of the center rod in the coupling region (middle or single rod) and along with the adjacent rods on both sides of the center rod (three rods), the output efficiency of Band I is reduced by 0.0367 and 0.183%, respectively. There is no such variation in Band II. The variation in normalized transmission spectra of single and three coupling rods is shown in Fig. 10a, b. The maximum output efficiency (85%) for Band I is observed when the radius of the coupling rod is 0.1 μm and it decreases from its maximum value when we vary the coupling rod radius. This may be due to improper coupling of signal between cavity and quasi waveguides (the coupling rods act as a resonant cavity at higher values of rod radius), and hence the signal power is reduced around the circular cavity.

4.4 Effect of lattice constant and rod radius

Here, three cases are considered to study the effect of lattice constant and rod radius. Firstly, both the variation of lattice constant and rod radius is treated as Case I and Case II represents the variation of lattice constant alone by keeping the rod radius as constant. Finally, Case III enumerates rod radius variation at fixed value of lattice constant.

Case I In general, the rod radius of the structure is defined as $r = x \times a$, where 'x' is the proposanality constant and 'a' is the lattice constant. It is obvious that the rod radius can be

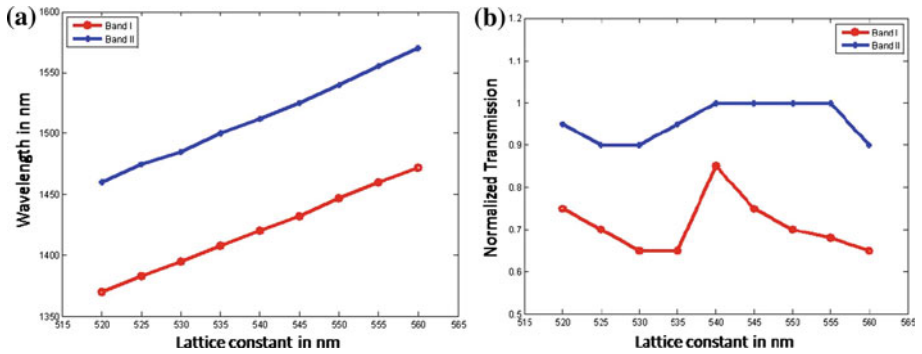

Fig. 11 Effect of **a** wavelength shift and **b** output efficiency while varying the rod radius and lattice constant

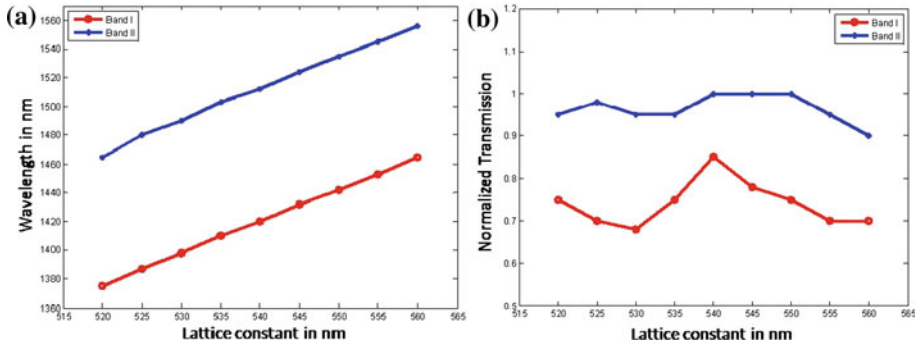

Fig. 12 Effect of **a** wavelength shift and **b** output efficiency while varying lattice constant

increased by increasing the lattice constant. If the lattice constant of the structure is increased (decreased), the resonant wavelength shifts towards higher wavelength (lower wavelength). It is observed that the rate of shift happens at 12.5 nm (approximately) for every 5 nm increase of lattice constant. The output efficiency is dropped while increasing the lattice constant as shown in Fig. 11a, b.

Case II By keeping the rod radius constant and varying the lattice constant with uniform step value, the variation of wavelength and output efficiency are shown in Fig. 12a, b. It is noted that approximately 11 nm wavelength shift for every 5 nm increase in lattice constant.

Case III By keeping lattice constant at one value and varying the rod radius linearly, the effects of changing the wavelength and normalized transmission are shown in Fig. 13a , b. It reveals that the wavelength shift depends on the rod radius and the output efficiency is maximum at 0.1 μm. In all cases, the maximum output efficiency observed at 0.1 μm of rod radius and 540 nm of lattice constant and hence they are used in the proposed structure.

4.5 Effect of number of rods in the structure

The number of rods in rows and columns around the circular ring resonator accounts this study. Initially, 7 columns of rods placed left and right side of the cavity and 5 rows of rods

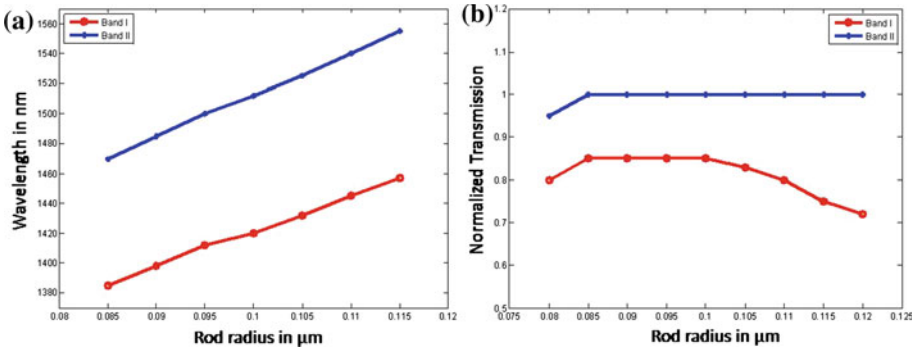

Fig. 13 Effect of **a** wavelength shift and **b** output efficiency while varying rod radius

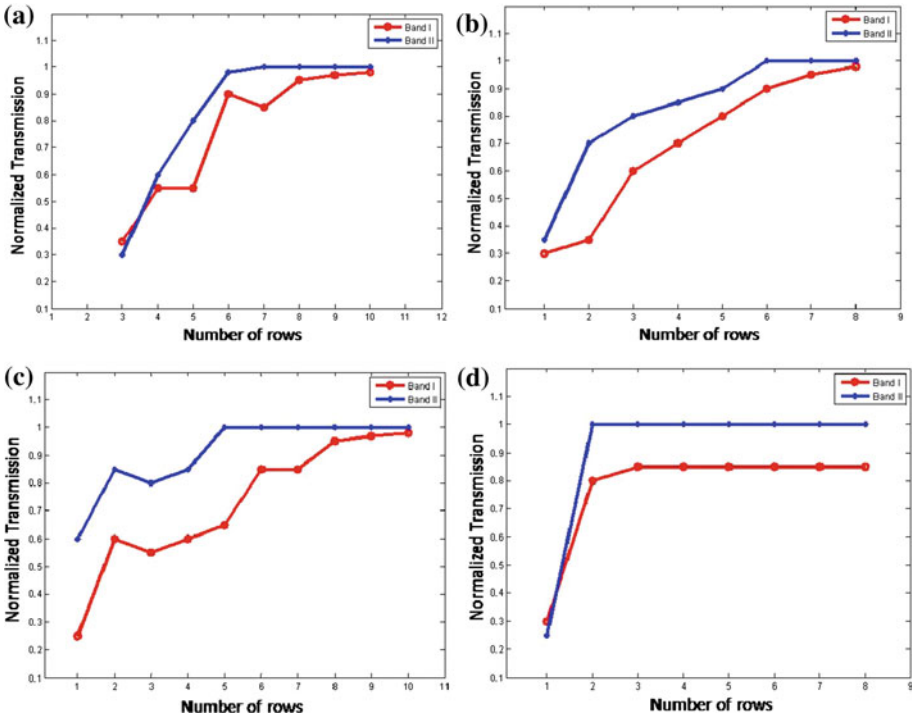

Fig. 14 Normalized transmission versus number of rods in the structure characteristics of **a** 10 columns and 8 rows of rods decreasing linearly in X and Z directions, **b** 8 columns and 8 rows of rods decreasing linearly in X and Z directions, **c** 10 columns of rods is decreasing linearly in X direction and 5 rows of rod is constant in Z direction and **d** 7 columns of rods is constant in X direction and 8 rows of rod is decreasing linearly in Z direction

positioned at top and bottom of the cavity are considered. The response of the transmission for varying the number of rods in the structure is shown in Fig. 14a–d. The filling of structure with rod is carried out either by adding or removing the number of rows and columns equally on all the four sides. It reveals that if the number of rows and columns around the cavity is decreased, the output efficiency and width of the bands are reduced. Better output efficiency

is obtained in both bands while increasing the number of rods in the structure. However, the bandwith is affected and the overall size of the structure also increases linearly.

Figure 14a depicts normalized transmission while varying the number of row of rods above (below) and number of columns of rods in right (left) side of the cavity from 5 and 7, respectively. In this case, the output efficiency of the filter is significantly improved when the rods in 'X' and 'Z' directions are above 7 and 5, respectively. Figure 14b shows the variation in two bands when the number of rods in 'X' and 'Z' directions are changed from 5. This is done for studying the effect of uniform size variation of the structure. Eventhough considerable efficiency is obtained at 6 rows and 6 columns of rods in 'X'and 'Z' directions, respectively, the width of the band is affected.

Five rows of rods are kept constant above (below) the cavity and the columns of rods in 'X' directions is varied lineally, which is shown in Fig. 14c. Similarly, the columns of rods in left and right side of cavity are kept 7 and the rods above and below the cavity are varied whose output spectrum is clearly shown in Fig. 14d. From the above study, the minimum required number of rows and columns of rods in 'X' and 'Z' directions is 7 and 5, respectively, to provide considerable output efficiency in both bands. To maintain the minimum size, the above said values are used in the proposed structure.

5 Conclusions

The circular Photonic Crystal Ring Resonator based BPF is designed and investigated. The output efficiency and resonant wavelength are examined by varying the radius of the coupling rod, the dielectric constant in the structure, reflector size, lattice constant, rod radius and number of rods in the structure. The output efficiency of PCBPF is, approximately, 100% over the range 1,504–1,521 nm and 85% at 1,420 nm with the bandwidth of 35 and 20 nm, respectively.

It is observed that increase in dielectric constant of the structure results in shifting the center wavelength to the higher wavelength by 9 nm for every 0.5 dielectric constant variation with trivial change in the bandwidth and vice versa. The number of periods in the reflector is kept '9' to ensure the maximum efficiency. While varying the radius of the single and three coupling rods from 0.06 to 0.14 μm, the output efficiency of Band I decreased by 0.0367 and 0.183% for every increase of 0.01 μm rod radius, respectively. The change in lattice constant or rod radius results in shifting of the resonant wavelength linearly. Also, it is noticed that their respective efficiencies are reduced for values other than 540 nm and 0.1 μm of lattice constant and rod radius. When the structure has minimum number of rods other than the reference, the output efficiency and bandwidth are affected; however, they are improved while increasing the number of rods in the structure. Also, increasing the number of rods in the structure leads to increase in overall size of the device and decreasing the bandwidth of operation. The overall dimension of the device is 11.4 μm $\times$10.2 μm, which is suitable for Photonic Integrated Circuits (PICs).

References

Berenger, J.P.: A perfectly matched layer for the absorption of electromagnetic waves. J. Comput. Phys. **114**, 185–200 (1994)

Chao, C., Li, X., Li, H., Xu, K., Wu, J., Lin, J.: Bandpass filters based on phase-shifted photonic crystal waveguide gratings. Opt. Express **15**, 11278–11284 (2007)

Costa, R., Melloni, A., Martinelli, M.: Band-pass resonant filters in photonic crystal waveguides. IEEE Photon. Technol. Lett. **15**, 401–403 (2003)
Djavid, M., Ghaffari, A., Monifi, F., Abrishamian, M.S.: Photonic crystal narrow band filters using biperiodic structures. J. Appl. Sci. **8**, 1891–1897 (2008a)
Djavid, M., Ghaffari, A., Monifi, F., Abrishamian, M.S.: T-Shaped channel drop filters using photonic crystal ring resonators. Phys. E **40**, 3151–3154 (2008b)
Ghaffari, A., Monifi, F., Djavid, M., Abrishamian, M.S.: Analysis of photonic crystal power splitters with different configurations. J. Appl. Sci. **8**, 1416–1425 (2008a)
Ghaffari, A., Monifi, F., Djavid, M., Abrishamian, M.S.: Heterostructure wavelength division demultiplexers using photonic crystal ring resonators. Opt. Commun. **281**, 4028–4032 (2008b)
Hwang, K.H., Song, G.H.: Design of a high-Q channel-drop multiplexer based on the two-dimensional photonic-crystal membrane structure. Opt. Express **13**, 1948–1957 (2005)
Joannopoulos, J.D., Meade, R.D., Winn, J.N.: Photonic Crystal: Modeling of Flow of Light. Princeton University Press, Princeton (1995)
Joannopoulos, J.D., Villeneuve, P.R., Fan, S.: Photonic crystals: putting a new twist of light. Nature **386**, 143–149 (1997)
John, S.: Strong localization of photons in certain disordered dielectric superlattices. Phys. Rev. Lett. **58**, 2486–2489 (1987)
Kok, A.A.M., Vander Tol, J.J.G.M., Roel, B., Smit, M.K.: Reduction of propagation loss in pillar-based photonic crystal waveguides. Journal of Lightwave Technology **27**, 3904–3911 (2009)
Lavrinenko, A., Borel, P.I., Frandsen, L.H., Thorhauge, M., Harpoth, A., Kristensen, M., Niemi, T., Chong, H.M.H.: Comprehensive FDTD modeling of photonic crystal waveguide components. Opt. Express **12**, 234–248 (2004)
Liu, T., Zakharian, A.R., Fallahi, M., Moloney, J.V., Mansuripur, M.: Design of a compact photonic-crystal based polarizing beam splitter. IEEE Photon. Technol. Lett. **17**, 1435–1437 (2005)
Manzacca, G., Paciotti, D., Marchese, A., Moreolo, M.S., Cincotti, G.: 2D photonic crystal cavity-based WDM multiplexer. Photon. Nanostruct. Fund. Appl. **5**, 164–170 (2007)
Moghaddam, M.K., Attari, A.R., Mirsalehi, M.M.: Improved photonic crystal directional coupler with short length. Photon. Nanostruct. Fund. Appl. **8**, 47–53 (2010)
Monifi, F., Djavid, M., Ghaffari, A., Abrishamian, M.S.: A new bandstop filter based on photonic crystals. In: Proceedings of PIER, Cambridge (2008)
Nozhat, N., Granpayeh, N.: Analysis and simulation of a photonic crystal power divider. J. Appl. Sci. **7**, 3576–3579 (2007)
Park, D.S., Park, S.G., Lee, E.H., Lee, S.G.: Photonic crystal-based GE-PON triplexer using point defects. Proc. SPIE **6897**, 689711 (2008). doi:10.1117/12.762186
Qiang, Z., Zhou, W., Soref, R.A.: Optical add-drop filters based on photonic crystal ring resonators. Opt. Express **15**, 1823–1831 (2007)
Robinson, S., Nakkeeran, R.: Channel drop filter based on 2D square-lattice photonic crystal ring resonator. In: 7th IEEE International Conference on WOCN'10, Colombo, 6–8 Sept (2010)
Robinson, S., Nakkeeran, R.: Investigation on two dimensional photonic crystal resonant cavity based bandpass filter. Optik optics (2011a, in press). doi:10.1016/j.ijleo.2011.05.004
Robinson, S., Nakkeeran, R.: Photonic crystal ring resonator based add-drop filter using hexagonal rods for CWDM systems. Optoelectron. Lett. **7**, 164–166 (2011b)
Shih, T.-T., Wu, Y.-D., Lee, J.-J.: Proposal for compact optical triplexer filter using 2-D photonic crystals. IEEE Photon. Technol. Lett. **21**, 18–21 (2009)
Wang, Q., Cui, Y., Zhang, H., Yan, C., Zhang, L.: The position independence of heterostructure coupled waveguides in photonic-crystal switch. Optik Optics **121**, 684–688 (2010)
Wang, C.-C., Chen, L.-W.: Channel drop filters with folded directional couplers in two-dimensional photonic crystals. Phys. B **40**, 1210–1215 (2010)
Yablonovitch, E.: Inhibited spontaneous emission on solid-state physics and electronics. Phys. Rev. Lett. **58**, 2059–2062 (1987)
Zabelin, V., Dunbar, L.A., Le Thomas, N., Houdre, R., Kotlyar, M.V., O'Faolain, L., Krauss, T.F.: Self-collimating photonic crystal polarization beam splitter. Opt. Lett. **32**, 530–532 (2007)